Theor Chim Acta (1994) 87: 343–371

Theoretica Chimica Acta

The phosphorescence of benzene obtained by *ab initio* and semi-empirical calculations*

S. Knuts[1], B. F. Minaev[2], H. Ågren[3], O. Vahtras[3]

[1] Department of Quantum Chemistry, University of Uppsala, P.O.B. 518, S-75120 Uppsala, Sweden

[2] Department of Chemistry, Cherkassy Engineering and Technological Institute, 257006, Cherkassy, Ukraine

[3] Institute of Physics and Measurement Technology, University of Linköping, S-58183, Linköping, Sweden

Received January 26, 1993/Accepted March 23, 1993

Summary. Radiative decay and phosphorescence of triplet stare benzene is doubly -orbital and spin- forbidden and is only activated through vibronic coupling among the manifold of triplet states. For this reason the determination of lifetime and transition moments for the decay of triplet benzene has posed a considerable challenge to both theory and experiment. In the present work we have addressed the triplet benzene problem at several levels of theory; by truncated perturbation theory and semiempirical, CNDO/S-CI, calculations; by complete sum-over-state calculations as implemented in recent *ab initio* multiconfiguration quadratic response (MCQR) theory; and by direct MCQR calculations of vibronic phosphorescence. The vibronic coupling is in the two former cases treated by the Herzberg–Teller (H–T) perturbation theory, involving four main mechanisms for the phosphorescent decay of triplet benzene. The results and interpretations given by these approaches as well as their merits and limitations are presented and discussed in some detail. Our calculations indicate that the phosphorescent decay of the $^3B_{1u}$ state takes place predominantly through vibronic coupling along the e_{2g} mode. We obtain a phosphorescence that is almost completely out-of-plane polarized, which is in line with more recent measurements by the microwave-induced delayed phosphorescence technique, and could reproduce quite well the intensity ratios for different vibronic bands obtained in that experiment. The final triplet state lifetime is the result of a delicate sum of contributions from several vibronic degenerate and non-degenerate modes. The direct vibronic phosphorescence calculations predict a long lifetime, about one minute – 68 seconds for the best wavefunction – and seem to focus on a doubling of the assumed, albeit not established, "best experimental" value for the radiative lifetime of triplet benzene; $\simeq$ 30 seconds.

Key words: Benzene – Phosphorescence – Decay

* Dedicated to Inga Fischer–Hjalmars on her 75th birthday

1 Introduction

For obvious reasons the characterization of excited states and spectra of the benzene molecule has formed an important research objective in quantum chemistry. The dipole spectrum of benzene was accordingly utilized in the earliest parametrizations and semi-empirical schemes, the first being the PPP model applied to benzene already in 1950 [1]. The historical account of the diversification of the PPP and other semi-empirical schemes to the application on spectra of aromatic compounds have been well documented, see e.g. a recent issue (No. 4, Vol 37) of the International Journal of Quantum Chemistry. Inga Fischer–Hjalmars made important contributions to the field of π-electron theory of heteroaromatic molecules. Her first investigation in this area, on the UV spectrum and electron distribution of aniline [2], was followed by a series of investigations of azabenzenes and other substituted benzenes [3, 4]. Much of this early work is fundamental for our understanding of the spectroscopy and electronic structure of excited states of aromatic compounds and has also served as a source of inspiration for later research on state-specific and propagator oriented *ab initio* approaches.

The development alluded to above refers primarily to singlet excited states. Although the important role of the low-lying triplet states for the description of solvation chemistry and spectroscopy of aromatic compounds has since long been recognized the number of theoretical investigations is very small in comparison with those on the singlet states. This follows from the simple fact that transitions to many of the lowest singlet states are dipole allowed and thus well characterized by absorption or fluorescence spectroscopy. On the theoretical side, it follows from the comparatively simple handling of the dipole interaction for singlet states that should be weighted against the nonlinear nature of the interaction, with simultaneous spin–orbit and dipole coupling, that is involved in the absorption or emission of triplet states. Calculations of triplet spectra have been hampered in a two-fold way; by the (correct) representation of the spin-orbit operator, and by the need to perform sum-over-state calculations to evaluate the perturbation expressions for phosphorescence and nonradiative yields. The convergence for such intermediate state summations is already slow for linear properties, and even more so for non-linear properties such as phosphorescence moments, where individual contributions of intermediate states are of arbitrary sign. The semi-empirical calculations have mostly dealt with finding acceptable approximations in both these aspects. On the other hand with recent progress in *ab initio* technology, calculations referring to both these aspects have been alleviated. We then refer to the efficient recursive evaluations of spin–orbit one- and two-electron integrals [5] and to the implementation of quadratic response formalisms for obtaining nonlinear molecular properties referring to arbitrary singlet and triplet perturbation operators [6].

Because of the obvious importance of benzene as a "benchmark" compound in theoretical aromatic chemistry it is ironic that both its singlet and triplet spectra have posed particular problems for *ab initio* calculations. In the singlet case the correct ordering of the lowest states was confirmed only by fairly recent calculations [7]. This difficulty has been referred to the description of the (different) degrees of ionizity of the excited π^* states and the accompanying dynamical polarization of the σ skeleton. In semi-empirical schemes this is to some extent accounted for by the parameterization, however, in state-by-state correlation calculations this description requires very large wavefunctions including simultaneous σ and π excitations. This has recently been discussed by Roos and co-workers

in a series of papers on CASPT2 and MRCI calculations of benzene, azabenzenes and nucleic acid base monomers [7, 8, 9].

In the triplet case the assignment of even the lowest state has been elusive. Although energy criteria from various computations are in agreement on a $^3B_{1u}$ assignment the spectral analysis has been ambiguous with respect to the symmetry character [10]. The assignment of the first excited triplet state in benzene as a $^3B_{1u}$ state was already suggested by Göppert–Mayer and Sklar [11] in 1938. Shull [12] and McClure [13] later refined the early experiments of Sklar [14]. Mizushima and Koide [15] made the first lifetime determination [15] (0.14 sec). McClure [13] introduced spin–orbit coupling in the analysis of the triplet states. The first actual calculation of the lifetime was conducted by Hameka and Oosterhoff, who reached a lifetime value of 190 sec, 3 orders of magnitude longer than the experimental value. Clementi [16] later refined lifetime predictions by means of spin–orbit coupling (SOC) calculations using sp^2 hybridized orbitals, and considered also two-center contributions to SOC elements, thereby obtaining a lifetime of 20 sec. However, Hameka and Oosterhof and Clementi considered states of different symmetry, $^3B_{2u}$ and $^3E_{1u}$, respectively, these also being different to the one ($^3B_{1u}$) originally assigned by Göppert–Mayer and Sklar. There was thus confusion which state should be assigned as the phosphorescent state. According to Kasha's rule this state should be the lowest among the triplet states.

Clues to the assignment problem were given by vibrational analysis of the benzene phosphorescence band. Many such analyses have been carried out trying to distinguish between $^3B_{2u}$ and $^3B_{1u}$ (or even $^3E_{1u}$ and $^3A_{2u}$) origin of the benzene phosphorescence. It was clear that the dipole transition is forbidden (0–0 transition is missing) and that emission is activated mostly by e_{2g} vibrations, however, a weak but significant activity of a b_{2g} vibration was also found [12, 17]. Nowadays it is well established that the lowest triplet state of the benzene molecule is $^3B_{1u}$. Basic to the benzene phosphorescence problem is the fact that the $\hat{a}^3B_{1u} \rightarrow \hat{X}^1A_{1g}$ transition is doubly forbidden by spin and orbital symmetry. Perturbation due to SOC alone cannot provide dipole-allowed character for the transition moment as is the case for other aromatic molecules with lower symmetry [18, 19]. This symmetry prohibition thus blocks the normal phosphorescence decay channel. Instead, the decay of the lowest triplet ($^3B_{1u}$) state is activated by vibronic interactions to the second triplet, the $^3E_{1u}$ state, which phosphoresces to the ground state. This implied that the expected lifetime of the lowest state is an order of magnitude longer than the lifetime of other $^3(\pi \rightarrow \pi^*)$ states in aromatic compounds. By introducing vibronic coupling through second order perturbation theory Albrecht [10] analyzed the vibronic interaction between the higher triplet states with the lowest $^3B_{1u}$ triplet state. Basing on polarization data as well as on energetic considerations Albrecht [10] also considered other routes to the triplet state lifetime of benzene, n.b. channels introduced by vibronic interaction with $^3A_{2u}$. These and the other mechanisms are computed and discussed below.

Calculations on the phosphorescence of benzene have exclusively been of semi-empirical type and have not considered all channels. Results have given rather different values for the radiative lifetime. The experiments have been undertaken with solvated benzene or with benzene matrix isolation, so the question of the true radiative (phosphorescent) lifetime of benzene has been considered open. In the present work we address the lifetime of triplet states of benzene both by means of *ab initio* and semi-empirical calculations. We employ the multiconfiguration quadratic response (MCQR) [6], respectively, CNDO/S-CI methods for this purpose. We perform calculations at three levels of theory: A) Semiempirical, CNDO/S-CI,

calculations using Herzberg–Teller perturbation theory for the vibronic coupling; B) *Ab inito* multi-configurational response calculations using Herzberg–Teller perturbation theory for the vibronic coupling; C) Direct *ab initio* multiconfigurational response calculations of vibronic phosphorescence.

2 Theory of phosphorescence

2.1 Ab initio theory: MCQR

The phosphorescence lifetime is determined from the rate of the spin–forbidden dipole transitions between two electronic states of different multiplicity. For a system with a singlet ground state S_0 and a first excited triplet state T_1, the unpolarized (average) transition rate is obtained by averaging initial states (triplet components) and summing over final states (photon polarizations and directions). The lifetime associated with the kth triplet component T_1^k is (in atomic units):

$$\frac{1}{\tau_k} = \frac{4\omega_1^3\alpha^3}{3} \sum_l |\langle S_0|x^l|T_1^k\rangle|^2 \tag{1}$$

where $\omega_1 = E(T_1) - E(S_0)$ is the frequency of the transition, α is the fine-structure constant and x^l is the lth component of the dipole operator. The total radiative lifetime (in the high-temperature limit) τ is obtained as $3/\tau = \Sigma_k 1/\tau_k$. The transition matrix element is determined from first-order perturbation theory as:

$$\langle S_0|x^l|T_1^k\rangle = \sum_s \frac{\langle S_0|x^l|S_s\rangle\langle S_s|H_{SO}^k|T_1^k\rangle}{E(T_1) - E(S_s)} + \sum_t \frac{\langle S_0|H_{SO}^k|T_t^k\rangle\langle T_t^k|x^l|T_1^k\rangle}{E(S_0) - E(T_t)} \tag{2}$$

where H_{SO}^k is the kth component of the spin–orbit operator. Cartesian triplet components are employed. These are related to the spherical components by:

$$T^x = \frac{T^{-1} - T^1}{\sqrt{2}} \tag{3}$$

$$T^y = i\frac{T^{-1} + T^1}{\sqrt{2}} \tag{4}$$

$$T^z = T^0 \tag{5}$$

In [20] it was demonstrated that the matrix element of Eq. (2) is associated with the residue of a quadratic response function:

$$\lim_{\omega \to \omega_1} (\omega - \omega_1) \ll x^l; H_{SO}^k, C \gg_{0,\omega} \tag{6}$$

where C is an arbitrary triplet operator.

As mentioned in the introduction, *ab initio* calculations of the kind presented here are made feasible by the efficient recursive evaluations of the full spin–orbit operator [5] and by the implementation of quadratic response formalisms [6] for obtaining non-linear response functions defined by Eq. (6). The electronic spin–orbit interaction constitutes the leading relativistic correction to the electrostatic interactions in a many-electron system [21]. In the Pauli approximation [22] it is represented by an operator of the form (in atomic units):

$$H_{SO} = \frac{\alpha^2}{2}\left[\sum_{iA} Z_A \frac{\mathbf{l}_{iA}\cdot\mathbf{s}_i}{r_{iA}^3} + \sum_{ij} \frac{\mathbf{l}_{ij}\cdot(\mathbf{s}_i + 2\mathbf{s}_j)}{r_{ij}^3}\right] \tag{7}$$

where i, j refer to electrons and A to nuclei. $\mathbf{r}_{ij}$ is the position of particle i relative to particle j and $\mathbf{l}_{ij} = \mathbf{r}_{ij} \times \mathbf{p}_i$ is the orbital angular momentum of particle i with respect to the position of particle j. The particle asymmetry in the two-electron part, the differing size of the spin-own-orbit and spin-other-orbit interaction, can be seen as a consequence of the Thomas precession [23], where α is the fine-structure constant. Relevant to mention for the present study is that this operator contains both one- and two-electron contributions and can be divided into one- and two-center parts. While the two-electron part (or one-center two-electron part) cannot be neglected; it is often accounted for by shielding of nuclear charges, the one-center approximation is cherished in semi-empirical as well as in "*ab-initio*" work.

The spin–orbit coupling (SOC) can thus be viewed as a perturbation of the non-relativistic Born–Oppenheimer Hamiltonian, the effect appearing as splittings of and transitions between the electrostatically determined electronic levels, for example between singlet and triplet states;

$$\langle {}^1\Psi \,|\, H_{SO} \,|\, {}^3\Psi(M_S) \rangle \tag{8}$$

where $\langle {}^1\Psi|$ is the singlet state and $\langle {}^3\Psi(M_S)|$ the M_S-component of the triplet state. In Ref. [5] it was shown how the SOC element can be calculated as the residues of the linear response function $\ll H_{SO}; H_{SO} \gg_{\omega=0}$. Such coupling constants between valence states may be obtained with the linear response method with a modest effort, only requiring that the singlet reference state is optimized. The SOC:s are then determined from a contraction of a gradient type vector with the spin–orbit operator and an eigenvector of the multiconfiguration linear response eigenvalue problem. The SOC:s between excited states can likewise be obtained from one sole ground state determination and from the quadratic response function, see e.g. [24]. Orbital relaxation is included through the orbital operators in the multiconfiguration linear response eigenvalue equation. Compared to optimizing separate MCSCF wavefunctions for the involved states, problems with non-orthogonal molecular orbitals are avoided. Compared to large scale CI calculations in a common orbital basis, the linear response method is competitive because much smaller configuration spaces are needed due to the inclusion of orbital relaxation in the response calculation.

The spin–orbit operator enters as one of the perturbing operators in quadratic response theory to describe phosphorescence. The implementation of quadratic response theory employed here is a generalization of quadratic response theory in [25] when there is no longer permutation symmetry in the two-electron integrals (as in spin–orbit integrals) and when the operators may both have singlet and triplet symmetry, and goes back to the formalism for quadratic response functions of Olsen and Jørgensen [20]. MCSCF reference wavefunctions are utilized, i.e. linear combinations of configuration state functions (CSF) $|0\rangle = \Sigma_g C_{g0} |\phi_g\rangle$, which in turn are constructed from Slater determinants $|\phi^D\rangle = \Pi_r a_r^\dagger |vac\rangle$ where $a_r^\dagger$ belong to an orthonormal set of spin–orbitals. The complement of the reference state is spanned by operators acting on the reference state. These operators may be orbital excitation operators:

$$q_i^\dagger = E(S)_{rs} \equiv a_{r\alpha}^\dagger a_{s\alpha} + S a_{r\beta}^\dagger a_{s\beta}; \quad r > s \tag{9}$$

where S is $+$ or $-$ for singlet and triplet orbital excitations, respectively, or state transfer operators $R_i^\dagger = |i\rangle\langle 0|$ which may create either a singlet or triplet excitation when operating on $\langle 0|$. These operators and their adjoints are collected in

a row vector:

$$\mathbf{T} = (q_i^\dagger \; R_i^\dagger \; q_i \; R_i) \tag{10}$$

and a general vector in this basis is written as a column vector:

$$N = \begin{pmatrix} \kappa_j \\ S_j \\ \kappa'_j \\ S'_j \end{pmatrix} \tag{11}$$

Thus N_j may refer either to an orbital rotation parameter or to a state transfer parameter (a CI-coefficient). In the phosphorescence case one considers $\mathbf{r}^{[1]}$, the dipole operator, and $\mathbf{H}_{SO}^{[1]}$, the spin–orbit operators as perturbing operators. The response function corresponding to the transition moment of Eq. (2) then reads [6] (Einstein summation convention):

$$\begin{aligned} \lim_{\omega \to \omega_1} (\omega - \omega_1) \ll x^l; H_{SO}^k, C \gg_{0,\omega} = & - N_j^r(\omega_f) H_{SO_{jl}}^{[2]} X_{lf} \\ & - N_j^{SO} (\mathbf{r}_{jl}^{[2]} + \mathbf{r}_{lj}^{[2]}) X_{lf} + N_j^r(\omega_f) \\ & \times (E_{jml}^{[3]} + E_{jlm}^{[3]} - \omega_f S_{jlm}^{[3]}) N_m^{SO} X_{lf}, \end{aligned} \tag{12}$$

the two linear response vectors $\mathbf{N}^r(\omega_f)$ and $\mathbf{N}^{SO}$ are obtained by solving the two linear response equations:

$$\mathbf{N}^r(\omega_f) = [(\mathbf{E}^{[2]} - \omega_f \mathbf{S}^{[2]})^{-1} \mathbf{r}^{[1]\dagger}]^\dagger \tag{13}$$

$$\mathbf{N}^{SO} = (\mathbf{E}^{[2]})^{-1} \mathbf{H}_{SO}^{[1]} \tag{14}$$

and the triplet excitation vectors (X_f) and frequencies (ω_f) are obtained from the solution of the MCSCF triplet excitation eigenvalue equation;

$$(\mathbf{E}^{[2]} - \omega_f \mathbf{S}^{[2]}) \mathbf{X}_f = 0 \tag{15}$$

These equations include several types of response matrices. The matrices $\mathbf{E}^{[2]}$ and $\mathbf{S}^{[2]}$ are the Hamiltonian and overlap matrices in the $\mathbf{T}$ operator basis.

$$E_{jk}^{[2]} = \langle 0 | [T_j^\dagger, [H_0, T_k]] | 0 \rangle \tag{16}$$

$$S_{jk}^{[2]} = \langle 0 | [T_j^\dagger, T_k] | 0 \rangle \tag{17}$$

The one-index matrices over the perturbing operators, with superscript "[1]", have the structure of MCSCF gradients and are therefore called gradient vectors and are defined as

$$\mathbf{r}_j^{[1]} = \langle 0 | [T_j^\dagger, r] | 0 \rangle \tag{18}$$

$$\mathbf{H}_{SO,j}^{[1]} = \langle 0 | T_j^\dagger, H_{SO}] | 0 \rangle \tag{19}$$

for the dipole and spin–orbit operators, respectively.

The two-index matrices with superscript "[2]" are defined similarly with double-commutator expressions. The three-index matrices are higher order generalizations of the two-index matrices. The important point is that they are never constructed explicitly, but are handled directly in matrix-vector products using direct CI techniques. By inspection of Eq. (12) the following four types of expressions are evaluated in case of phosphorescence i) $\mathbf{E}^{[3]}$ times two vectors; ii) $\mathbf{S}^{[3]}$ times two vectors; iii) $\mathbf{r}^{[2]}$ times a vector, and; iv) $\mathbf{H}_{SO}^{[2]}$ times a vector.

The computationally dominant operation is evidently the first of these four contractions, the one which contracts a third-order Hessian type matrix with two response vectors. It is clear that this operation must be conducted directly, with an MCSCF wavefunction of 10^5 parameters (vector length of $2 \cdot 10^5$) $E^{[3]}$ contains 10^{15} elements, something impossible to store. The explicit expressions are lengthy, and are given in [6]. We only note here that the key entries in these equations all contain gradient vectors of operators. These operators may be singly or doubly one-index transformed. The one-index transformation is another key operation of the theory, and constitutes the basic cause for making the direct transformation above at all possible. For instance the unperturbed Hamiltonian H_0:

$$H_0 = \sum_{rs} h_{rs} E(+)_{rs} + \tfrac{1}{2} \sum_{pqrs} (rs|tu) e(+,+)_{rstu}, \tag{20}$$

are expressed as one-index transformed:

$$H_0({}^b\kappa) \equiv \left[\sum_{rs}^{b} \kappa_{rs} E(S_b)_{rs}, H_0 \right] \tag{21}$$

i.e. evaluated over one-index transformed integrals referring to orbital rotation vectors ${}^b\kappa$, and as doubly one-index transformed:

$$H_0({}^b\kappa, {}^c\kappa) \equiv \left[\sum_{rs}^{c} \kappa_{rs} E(S_c)_{rs}, \left[\sum_{tu}^{b} \kappa_{tu} E(S_b)_{tu}, H_0 \right] \right] \tag{22}$$

i.e. evaluated over integrals which are one-index transformed both with respect to ${}^b\kappa$ and ${}^c\kappa$. (In the phosphorescence case "b" refers to the dipole, and "c" to the spin–orbit operator). The explicit expression for these integrals can be found in [6]. In a recent work [26] it is shown how these one-index transformations can be carried out efficiently without pre-transforming or storing the integrals. The excitation operators entering these expressions are defined as in [27]:

$$E(S)_{pq} = a^{\dagger}_{p\alpha} a_{p\alpha} + S a^{\dagger}_{p\beta} a_{q\beta} \tag{23}$$

$$e(S_1, S_2)_{pqrs} = E(S_1)_{pq} E(S_2)_{rs} - E(S)_{ps} \delta_{rq} \tag{24}$$

S has the same meaning as in Eq. (9); $+$ for singlet and $-$ for triplet (satisfying $S = S_1 S_2$);

The gradients entering the expressions for direct transformations can be divided into orbital gradients:

$$F_{pq} = \langle L | [E(S_g)_{qp}, H(S_1, S_2)] | R \rangle \tag{25}$$

and CI gradients;

$$\langle j | H(S_1, S_2) | R \rangle \tag{26}$$

where $H(S_1, S_2)$ is the general two-electron operator:

$$H(S_1, S_2) = \sum_{pq} f_{pq} E(S)_{pq} + \sum_{pqrs} g_{pqrs} e(S_1, S_2)_{pqrs} \tag{27}$$

or in special cases a one-electron operator. f denotes here any one-electron integral and g any two-electron integrals over the Hamiltonian or any observables. They may also refer to one-index transformed integrals. The orbital type gradients are expanded in terms of generalized Fock and "Q"-matrices commonly employed in MCSCF theory [28, 29] (but with differential permutational symmetry of indices),

the CI-gradient are computed using the determinant-based direct technique of Olsen et al. [30]. The advantage of using a determinant-based formalism is that alpha and beta spins can be treated separately which reduces the dimensionality of the problem considerably.

2.2 *Semi-empirical theory for vibronic and spin–orbit coupling: CNDO/S-CI*

An extensive semi-empirical analysis of the benzene phosphorescence problem accounting for SOC and vibronic perturbations was presented in [31] and [32]. We outline here a CNDO type analysis taking into account the vibronic solutions obtained in [31]. In a semiquantitative manner the present analysis coincides with that of Albrecht [10]. In the Herzberg–Teller approximation the dependence of the electronic wavefunction on nuclear configuration Q has the form [31, 33]:

$$\Psi_n(r, Q) = \Psi_n(r, Q_0) + \sum_{m \neq n,\, \alpha} \frac{J^{\alpha}_{mn} Q_{\alpha}}{E_n - E_m} \Psi_m(r, Q) \tag{28}$$

where

$$J^{\alpha}_{mn} = \langle \Psi_m(r, Q_0) \left[\frac{\partial}{\delta Q_{\alpha}} \left(\sum_{i,A} \frac{Z_A}{r_{iA}} \right) \right]_0 \Psi_n(r, Q) \rangle \tag{29}$$

$\Psi_n(r, Q)$ denotes the electronic part of the Born–Oppenheimer (BO) wavefunction:

$$\Phi_{n\mu}(r, Q) = \Psi_n(r, Q) X_{n\mu}(Q) \tag{30}$$

and $X_{n\mu}(Q) = \Pi_{\alpha} \chi^{\alpha}_{n\mu}(Q_{\alpha})$ is the vibrational wavefunction in form of a product of harmonic oscillator eigenfunctions $\chi^{\alpha}_{n\mu}$: μ is a vibrational quantum number. In the equations given above Q_0 denote the equilibrium geometry, Q_{α} the particular type of vibronic normal mode with α running from 1 to 3N-6, r the electronic variables, and Z_A denotes a core charge of atom A in the CNDO approximation.

Roche and Jaffé have shown that $\Psi_n(r, Q_0)$ is a bad zeroth-order wavefunction for $\Psi_n(r, Q)$ in the CNDO approximation, because if only the 1s AO follows the nuclei, the field exerted on the nuclei is going to be too strong and therefore, the shape of the approximate BO potential surface is expected to be much too sharp [33]. In order to avoid this difficulty Roche and Jaffé used the zeroth-order wavefunction $\Psi'_n(r, Q)$ in which all the coefficients of the MOs are the same as in $\Psi_n(r, Q_0)$, but in which the AO follow the nuclei. The matrix element (29) can now be written in the form:

$$J^{\alpha}_{mn} = \left[\frac{\partial}{\partial Q_{\alpha}} \langle \Psi'_m(r, Q) | H | \Psi'_n(r, Q) \rangle \right]_0 \tag{31}$$

where H is the exact electronic Hamiltonian. Calculating Eq. (31) we must take into account that at $Q \neq Q_0$ the MOs are not self-consistent any more and Brillouin's theroem does not hold. So the general expressions for CI matrix elements must be differentiated. For the triplet states the following formulas have

been obtained [31, 33]:

$$J^{\alpha}_{mn} = \sum_{i-a}\sum_{j-b} {}^3V_{ia,m}\,{}^3V_{jb,n}\left[\delta_{ij}\left(\frac{\partial F_{ab}}{\partial_{ab}Q_\alpha}\right)_0 - \delta_{ab}\left(\frac{\partial F_{ij}}{\partial Q_\alpha}\right)_0 + \sum_{A,B} D^A_{ij}D^B_{ab}\frac{a_0}{e^2}\gamma^2_{AB}\left(\frac{\partial R_{AB}}{\partial Q_\alpha}\right)_0\right] \tag{32}$$

where

$$D^A_{ij} = \sum_{\mu} c^A_{i\mu}c^A_{j\mu} \tag{33}$$

and

$$\left(\frac{\partial F_{ij}}{\partial Q_\alpha}\right)_0 = \tfrac{1}{2}\sum_{\mu,\nu} c_{i\mu}c_{j\nu}(\beta^0_\mu + \beta^0_\nu)\left(\frac{\partial S_{\mu\nu}}{\partial Q_\alpha}\right)_0 - \frac{a_0}{e^2}\gamma^2_{AB}\left[\sum_k\sum_{AB}(2D^A_{ij}D^B_{kk} - D^A_{ik}D^B_{jk}) - \sum_A\sum_{B\neq A} D^A_{ij}Z_B\right]\left(\frac{\partial R_{AB}}{\partial Q_\alpha}\right)_0 \tag{34}$$

Here γ_{AB} are the coulomb repulsion integrals calculated by Mataga–Nishimoto approximation [34].

In CNDO/S-CI we consider single excitations:

$${}^\lambda\Psi_n = \sum_{i-a} {}^\lambda V_{ia,n}\,{}^\lambda\Psi_{i-a}, \quad \lambda = 2s+1, M_s = 0 \tag{35}$$

from SCF closed-shell ground state Ψ_0: i, j, k – are doubly occupied MOs in singlet ground state; a, b-unoccupied MOs:

$${}^{3,1}\Psi_{i-a} = \frac{1}{\sqrt{2}}(|\psi_1\bar{\psi}_1\cdots\psi_i\bar{\psi}_\alpha| \pm |\psi_1\bar{\psi}_1\cdots\bar{\psi}_i\psi_a|); \quad M_s = 0, \tag{36}$$

where $\psi_i = \Sigma_{\mu,A}c^A_{i\mu}\phi^A_\mu$ is an LCAO-MO in a minimal STO basis set. The force field for the benzene molecule was taken from [35]. For the BO wavefunctions (28)–(30) the transition moment between an electronically excited state n with zero-vibrational level $\Phi_{n0}(r, Q)$ and the electronic ground state with μ-vibrational excited level $\Phi_{0\mu}(r, Q)$, is equal to:

$$\mathbf{M}^{0\mu}_{n0} = \mathbf{M}_{n0}(Q_0)\int X_{n0}X_{0\mu}dQ + \sum_\alpha \boldsymbol{\eta}_{n0,\alpha}\int X_{n,0}Q_\alpha X_{0\mu}dQ \tag{37}$$

where

$$\mathbf{M}_{n0}(Q) = \langle\Psi_n(r, Q)|\sum_i \mathbf{r}_i|\Psi_0(r, Q)\rangle \tag{38}$$

$$\boldsymbol{\eta}^\alpha_{n0} = \left[\frac{\partial}{\partial Q_\alpha}\mathbf{M}_{n0}(Q)\right]_0 \tag{39}$$

In the harmonic approximation the first term in Eq. (37) determines the (0, 0) band if the transition is not forbidden by symmetry. The second term is different from zero if μ is excited in Q_α by one vibrational quanta. In this case $\int\chi^\alpha_{n0}Q_\alpha\chi^\alpha_{0\mu}dQ = (h/8\pi^2\nu_\alpha)^{1/2}$ and the vibronic $0\to 1$ transition intensity is determined by Eq. (39). Neglecting the vibronic mixing with the singlet ground state

we obtain:

$$\eta^{\alpha}_{n0} = \sum_{m \neq n} \frac{J^{\alpha}_{mn}}{E_n - E_m} \mathbf{M}_{m0}(Q_0) \tag{40}$$

Intensities of spin-allowed singlet vertical transitions in CNDO/S-CI approximation are determined by:

$$^1\mathbf{M}_{n0} = \sqrt{2} \sum_{ia} {}^1V_{i\alpha, n} \mathbf{q}_{ia} \tag{41}$$

where $\mathbf{q}_{ia} = \langle \psi_1 | \mathbf{r} | \psi_a \rangle$; for example, the x-projection of $\bar{q}_{ia}$ is equal to (in a.u.):

$$q^x_{ia} = \sum_A \left[D^A_{ia} x_A + \frac{5}{\sqrt{3} Z'_A} (C^A_{si} C^A_{xa} + C^A_{xi} C^A_{sa}) \right] \tag{42}$$

here Z'_A is the Slater effective charge and x_A the x coordinate of atom A. The triplet–triplet transition moments from the higher triplets $^3\Psi_p$ to the lowest triplet state $^3\Psi_1$ are determined by the relation:

$$^3\mathbf{M}_{p1} = \sum_{ab} \mathbf{q}_{ab} \sum_i {}^3V_{ia, p} \, {}^3V_{ib, 1} - \sum_{ij} \mathbf{q}_{ij} \sum_a {}^3V_{ia, p} \, {}^3V_{ja, 1} \tag{43}$$

For studying the intensity of the S–T transition we must take into account the SOC effect. In the framework of the CNDO method the natural approximation, like the previous vibronic one presented in [33], is an effective one-electron model [31]:

$$H_{SO} = \sum_A \zeta_A \sum_i \mathbf{l}_{iA} \cdot \mathbf{s}_i \tag{44}$$

The reasons of this approximation have been discussed and illustrated by SOC calculations in diatomic and triatomic molecules [31]. The SOC matrix elements for CI with single excitations are equal to [32]:

$$\langle {}^3\Psi^u_p | H_{SO} | {}^1\Psi_0 \rangle = -\frac{1}{\sqrt{2}} \sum_{i-a} {}^3V_{i-a, p} B^u_{ai} \tag{45}$$

$$\langle {}^3\Psi^u_p | H_{SO} | {}^1\Psi_n \rangle = \tfrac{1}{2} \left[\sum_{i-a} \sum_{j-a} {}^3V_{ja, p} \, {}^1V_{ia, n} B^u_{ji} - \sum_{i-a} \sum_{j-b} {}^3V_{ib, p} \, {}^1V_{ia, n} B^u_{ba} \right] \tag{46}$$

where orbital integrals $\mathbf{B}_{ji} = \langle \Psi_j | \mathbf{B} | \Psi_i \rangle$ are determined as follows in one-center approximation.

$$B^x_{ji} = \sum_A \zeta_A (C^A_{zj} C^A_{yi} - C^A_{yj} C^A_{zi}) \tag{47}$$

$$B^y_{ji} = \sum_A \zeta_A (C^A_{xj} C^A_{zi} - C^A_{zj} C^A_{xi}) \tag{48}$$

$$B^z_{ji} = \sum_A \zeta_A (C^A_{yj} C^A_{xi} - C^A_{xj} C^A_{yi}) \tag{49}$$

The triplet configurations are determined here as spin–functions of zero-field (3)–(5). The T–S phosphorescence transition moment in the first order perturbation theory is now equal to:

$$\bar{M}^u_{10} = \langle {}^3\Psi^u_1 | \mathbf{M} | {}^1\Psi_0 \rangle = \sum_{n \neq 0} G^u_{1n} \, {}^1\mathbf{M}_{n0} - \sum_{p \neq 1} G^u_{p0} \, {}^3\mathbf{M}_{p1} + G_{10} ({}^3\mathbf{M}_{00} - {}^3\mathbf{M}_{11}) \tag{50}$$

where

$$G_{p0}^{u} = \frac{\langle {}^3\Psi_p^u | H_{SO} | {}^1\Psi_0 \rangle}{{}^3E_p - {}^1E_0} \tag{51}$$

The difference of permanent dipole moments of the ground singlet and first triplet states (the last term in Eq. (50)) is relevant for a direct vibronic calculation of the phosphorescence lifetime of benzene. We have performed this direct calculation of $M_{10}^{x,y}$ by the CNDO/S-CI method by Eqs. (45–51) for three points along the normal coordinate of the b_{2g} vibration ($\nu_4 = 703\ \mathrm{cm}^{-1}$, see discussion below) which is followed by a numerical estimation of the derivative $\bar{\eta}_{10}^{\alpha} = (\partial \mathbf{M}_{10}^{x}/\partial Q_{\alpha})_0$ and vibronic intensity calculation for the $(v' = 0) \rightarrow (v'' = 1)$ transition in the ${}^3B_{1u} \rightarrow {}^1A_{1g}$ emission spectrum by Eq. (37). The oscillator strength for this transition was estimated to $3 \cdot 10^{-11}$. We have also performed these direct calculations at the *ab initio* MCQR level for the most important vibrational modes. These results are discussed in the next section. We shall start the discussion of the results obtained by the vibronic theory of Herzberg–Teller type (28)–(40). The vibronic mixing of Eq. (28) of the lowest triplet ${}^3B_{1u}$ state with the $1{}^3E_{1u}$ and $1{}^3A_{2u}$ states calculated on the CNDO/S-CI level (32)–(34) will be used in subsequent estimation of the phosphorescence lifetime through calculations of the ${}^3E_{1u} \rightarrow {}^1A_{1g}$ and ${}^1A_{2u} \rightarrow {}^1A_{1g}$ transition intensities by the SOC treatment in the CNDO/S-CI (41)–(51) and MCQR (6)–(27) approaches.

3 The Herzberg–Teller treatment of benzene phosphorescence

In order to put the coming discussion into context we recapitulate in this section briefly the basic facts about phosphorescence in benzene.

The benzene phosphorescence spectrum in rigid glasses reveals a dominant vibronic activity of the ν_8 ($1602\ \mathrm{cm}^{-1}$) and ν_9 ($1174\ \mathrm{cm}^{-1}$) e_{2g} vibrations. The ν_6 ($606\ \mathrm{cm}^{-1}$) mode is very active in fluorescence (${}^1B_{2u} \rightarrow {}^1A_{1g}$), but appears very weakly in the phosphorescence spectrum [17, 12]. The e_{2g} intensity is uniformly polarized out-of-plane with approximately 70% [10]. The b_{2g} vibration ν_4 ($703\ \mathrm{cm}^{-1}$) appears weakly [17, 12] and shows predominantly in-plane polarization of phosphorescence emission [10]. There are four e_{2g} in-plane and two out-of-plane b_{2g} normal modes in benzene which are relevant for the vibronic activity.

A triplet state acquires singlet character, leading to dipole radiation, by 1) spin–orbit coupling, 2) spin–vibronic coupling, 3) spin–orbit coupling with vibronic coupling in the singlet manifold, and 4) vibronic coupling in the triplet manifold with spin–orbit coupling. The implication of this for phosphorescence of benzene are the following detailed mechanisms, denoted I, II, III and IV, and represented pictorially in Fig. 1.

Mechanism I.
Vibronic coupling between ${}^3B_{1u}$ and ${}^3E_{1u}$ through the e_{2g} mode, followed by dipole coupling (M^z) between ${}^3E_{1u}$ and ${}^3E_{1g}$ and spin–orbit coupling ($H_{SO}^{x,y}$) between ${}^3E_{1g}$ and the ground state.

Mechanism II.
Vibronic coupling between ${}^3B_{1u}$ and ${}^3E_{1u}$ through the e_{2g} mode, followed by spin–orbit coupling ($H_{SO}^{x,y}$) between ${}^3E_{1u}$ and ${}^1A_{2u}$ and dipole coupling (M^z) between ${}^1A_{2u}$ and the ground state.

Mechanisms for phosphorescence of benzene:

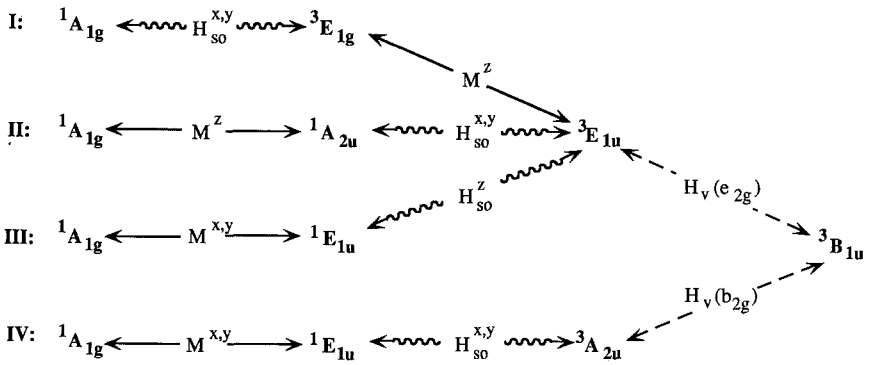

Fig. 1. The four different mechanisms of benzene phosphorescence

Mechanism III.
Vibronic coupling between $^3B_{1u}$ and $^3E_{1u}$ through the e_{2g} mode, followed by spin–orbit coupling (H_{SO}^z) between $^3E_{1u}$ and $^1E_{1u}$ and dipole coupling ($M^{x,y}$) between $^1E_{1u}$ and the ground state.

Mechanism IV.
Vibronic coupling between $^3B_{1u}$ and $^3A_{2u}$ through the b_{2g} mode, followed by spin–orbit coupling ($H_{SO}^{x,y}$) between $^3A_{2u}$ and $^1E_{1u}$ and dipole coupling ($M^{x,y}$) between $^1E_{1u}$ and the ground state.

These mechanisms are also represented in singlet and triplet level diagrams in Fig. 2, which also indicate the spin-sublevels of the triplet states. It should be pointed out that the response theory formulation represents these mechanisms in a general way in that the interaction between the singlet and triplet manifolds include all states of the specified symmetry and not only a particular state, e.g. the lowest state of that symmetry as given in Figs. 1 and 2.

3.1 CNDO/S-CI results

First we have studied the vibronic mixing in the triplet manifold. It appears that the $^3B_{1u}$ and $^3E_{1u}$ coupling by e_{2g} vibrations is most efficient and the summation in Eq. (28) for the e_{2g} modes can be restricted to these two degenerate $^3E_{1u}$ states. The result is in a good agreement with previous theories [10]. The b_{2g} vibrations are not so active: for ν_4 (703 cm^{-1}) we have obtained the largest mixing between $^3B_{1u}$ and $^3A_{2u}$ states. The last one has a comparatively low energy 6.39 eV and was claimed not to be an artifact of the CNDO/S-CI method [32]. Vibronic coupling in the singlet manifold is most efficient for $^1B_{2u}$ and $^1B_{1u}$ mixing with the $^1E_{1u}$ state by e_{2g} vibrations as has been established earlier [10, 33] but it does not contribute to the phosphorescence in the simple CNDO approximation of Eq. (44). Hameka and Oosterhoffs [36] calculation of SOC between $\pi\pi^*$ states $^1B_{2u}$ and $^3B_{1u}$ showed that the SOC gives a negligible contribution to the $^3B_{1u} \rightarrow {}^1A_{1g}$ transition moment, when the observed intensity of $^1B_{2u} \rightarrow {}^1A_{1g}$ transition is taken into account as

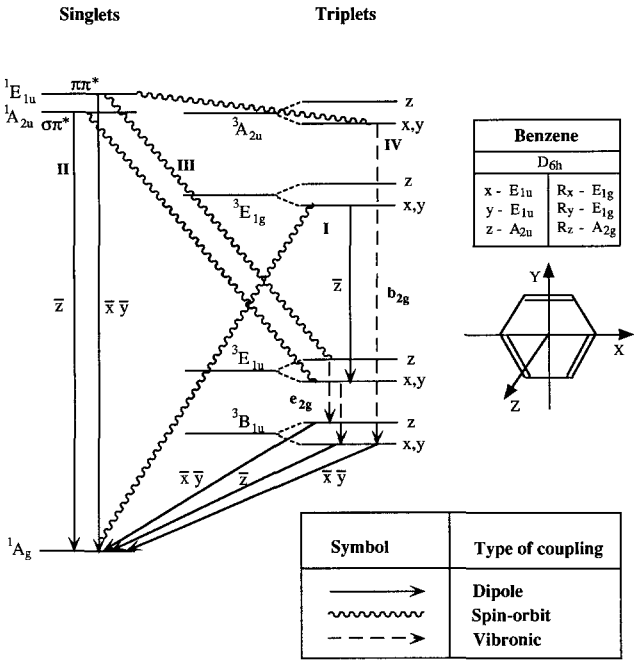

Fig. 2. Scheme for the different phosphorescence mechanisms in the triplet and singlet manifolds

borrowing from the $^1E_{1u} \rightarrow {}^1A_{1g}$ transition by the e_{2g} ($\nu_6 = 606\ \mathrm{cm}^{-1}$) perturbation. The problem of $^3B_{1u}$ phosphorescence reduces mainly to the problem of $^3E_{1u} \rightarrow {}^1A_{1g}$ transition intensity. The total e_{2g} intensity contribution is determined by the final relation:

$$\langle {}^3B_{1u}^{x,y}|z|{}^1A_{1g}\rangle = 0.375\langle {}^3E_{1u}^{x,y}|z|{}^1A_{1g}\rangle \tag{52}$$

where the most active mode is the ν_8 vibration ($1601\ \mathrm{cm}^{-1}$). It contributes with 77% to the total e_{2g} intensity which is in good agreement with the experiment [10]. The contributions from the other e_{2g} vibrations are, correspondingly, equal to 18% ($\nu_6 = 606\ \mathrm{cm}^{-1}$), 4.5% ($\nu_9 = 1178\ \mathrm{cm}^{-1}$) and 0.5% ($\nu_7 = 3056\ \mathrm{cm}^{-1}$) [31]. The second triplet–singlet transition moment ($^3E_{1u}$–$X\,{}^1A_{1g}$) in the benzene molecule has earlier been calculated by Mizushima and Koide [37], Clementi [16] and Veeman and Van der Waals [38] basing on simple assumptions of the nature of σ–$\pi^*(^1A_{2u})$ excited states which perturb the $^3E_{1u}$ state through SOC and which submit the main intensity, polarized perpendicular to the plane of the molecule. They used localized C–C and C–H (nonpolarized) σ-bonds, with wavefunctions constructed from sp^2-AO's and used arbitrary assumptions about the energy of the $^1A_{2u}$ states. Only one, $^1A_{2u}$ $\sigma(e_{2g}) \rightarrow \pi^*(e_{2u})$, state was then taken into account [16, 37].

CNDO/S-CI calculations show that the first $X\,{}^1A_{1g}$–$^1A_{2u}$ transition ($3e_{2g}$ $-1e_{2u}$ excitation) with low energy (6.4 eV) and low oscillator strength ($f = 0.001$) produces a very small contribution to M_{20}. The $^3E_{1u}$–$X\,{}^1A_{1g}$ transition moment [31, 32] is only $1.6 \cdot 10^{-6}$ a.u. because of a non-efficient SOC ($\langle 1\,{}^1A_{2u}|H_{SO}|{}^3E_{1u}\rangle$ $= 0.51\ \mathrm{cm}^{-1}$). In a simple sp^2-hybrid approximation it was $2.23\ \mathrm{cm}^{-1}$, and $f(^1A_{2u}$–$^1A_{1g}) = 2.86 \cdot 10^{-2}$ for $E(^1A_{2u}) = 8$ eV (from assumption) [16]. CNDO/SCI results [31] show, see Table 1, that besides the first $1\,{}^1A_{2u}$ state there are many other

contributions and many of them have opposite signs. So the problem of the transition moment $\langle {}^3E_{1u}|z|X^1A_{1g}\rangle$ is a problem of a rather delicate balance between many oscillating perturbations of the $^1A_{2u}$ and $^3E_{1g}$ states. In CNDO/S-CI it is easy to solve the problem for the single excitations directly accounting for all contributions. In more sophisticated *ab initio* methods the problem of convergence of the perturbation theory expansion must be carefully taken into account, as is accomplised by the MCQR methodology.

Table 1 shows results for the doubly degenerate $^3E_{1u}$ state with x- and y-spin sublevel components both being active in the out-of-plane z-polarized emission. Both components have an oscillator strength $f(^3E^{x,y}_{1u} \rightarrow X^1A_{1g}) = 0.187 \cdot 10^{-8}$, where the energy $E(^3E_{1u}) = 4.5$ eV is taken from experiment (CNDO/S-CI gives 3.0 eV and 4.1 eV for the $^3B_{1u}$ and $^3E_{1u}$ states, respectively). The radiative phosphorescence lifetime of the $^3E_{1u}$ state has no physical meaning and cannot be measured because this energy is quenched through vibrational relaxation to the first triplet state, $^3B_{1u}$, which produces the observed benzene phosphorescence at 3400 Å (3.66 eV). Using the above-mentioned CNDO/S-CI calculated vibronic activity for e_{2g} vibrations, see Eq. (52), we have the transition moment:

$$\langle {}^3B^{x,y}_{1u}|z|X^1A_{1g}\rangle = 0.4886 \cdot 10^{-4} \text{ a.u.} \tag{53}$$

and the oscillator strength $f^x_{01} = f^y_{01} = 2.14 \cdot 10^{-10}$. This corresponds to the radiative lifetime of x and y spin sublevels $\tau_x = \tau_y = 1.5/\nu^2 f = 8.0$ s.

The mechanism III gives an e_{2g}-vibronic intensity with in-plane polarization. In the CNDO approximation this intensity is forbidden. Using estimations [16, 36] $\langle {}^3E^z_{1u}|H_{SO}|{}^1E_{1u}\rangle = 0.4 \text{ cm}^{-1}$ we get:

$$(M^z_{10})^y = (M^z_{10})^x = \langle {}^3B^z_{1u}|x|{}^1A_{1g}\rangle = 1.88 \cdot 10^{-5} \text{ a.u.} \tag{54}$$

which corresponds to the oscillator strength $f^z_{10} \cong {}^2\Pi^{15}\,\Pi^{0-11}$ for the z-spin sublevel.

Studying the mechanism IV we have found that only the 1^3A_{2u} state gives a large contribution:

$$\langle {}^1E_{1u}|H_{SO}|{}^3A^{x,y}_{2u}\rangle = 0.47 \text{ cm}^{-1} \tag{55}$$

Table 1. Calculation of electric dipole transition moment $\langle {}^1A_{1g}|z|{}^3E^x_{1u}\rangle$ by the CNDO/S-CI method for mechanisms I and II

n	$^\lambda\Psi_n$	$^\lambda E_n$ [eV]	$^\lambda M^z_{n,m}$ [a.u.]	$\langle H_{so}\rangle$ [cm^{-1}]	$\langle M^x_{02}\rangle^z_n$ [10^{-4} a.u.]
1	$^1A_{2u}$	6.39	− 0.062	0.51	0.0161
2	$^1A_{2u}$	10.08	0.892	5.837	− 1.0562
3	$^1A_{2u}$	13.50	1.028	− 6.495	0.5954
4	$^1A_{2u}$	17.56	− 0.253	− 2.962	− 0.8920
1	$^3E_{1g}$	8.06	0.102	23.705	− 0.3757
2	$^3E_{1g}$	9.14	− 0.614	− 0.037	− 0.0030
3	$^3E_{1g}$	10.46	− 0.266	− 8.295	− 0.2634
4	$^3E_{1g}$	10.61	0.166	3.950	− 0.0767
5	$^3E_{1g}$	12.07	− 0.276	− 8.193	− 0.2317
6	$^3E_{1g}$	24.93	− 0.697	5.231	0.1814
$\Sigma_n(^1A_{2u}, E_{1g})$					− 1.3030

which corresponds to a transition moment of:

$$\langle {}^3A_{2u}|x|{}^1A_{1g}\rangle = 2.19\cdot 10^{-4}\ \text{a.u.} \tag{56}$$

The ${}^3A_{2u}$ and ${}^1E_{1u}$ states are nearly degenerate and their energy difference is a crucial value. Vibronic calculations show that the b_{2g} vibrational mode $\nu_4 = 703\ \text{cm}^{-1}$ is the most active one and finally we obtain:

$$\langle {}^3B^x_{1u}|x|{}^1A_{1g}\rangle = 0.07\langle {}^3A^x_{2u}|x|{}^1A_{1g}\rangle \tag{57}$$

We find that the mechanism IV produces the in-plane polarized b_{2g} vibronic band in the benzene phosphorescence from x- and y-spin sublevels with the oscillator strengths $f^x_{01} = f^y_{01} = 1.7\cdot 10^{-11}$. The intensity is an order of magnitude smaller

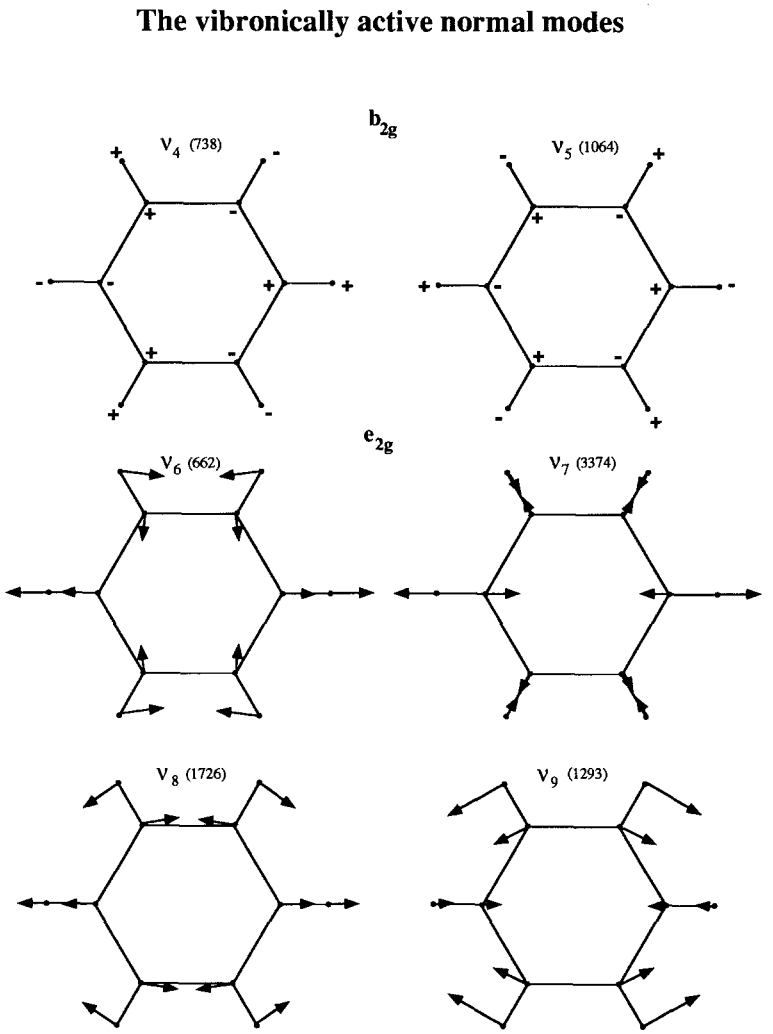

Fig. 3. A display of the different vibronic active modes for the phosphorescence mechanisms in benzene

for the b_{2g}-bands than for the e_{2g}-bands in benzene phosphorescence as predicted by the CNDO/S-CI method.

3.2 MCQR results

3.2.1 Computational details. The basis sets employed in the MCQR calculations are the same as in previous calculations on singlet and triplet spectra of azabenzenes [39, 40]. These are the Double Z (DZ) and Triple (TZ) basis sets of Dunning [41, 42] and the TZP and TZPD basis sets constructed by Sadlej [43], which are compact triple zeta basis sets (C:5*s*3*p*;H:3*s*) with polarizing functions (*P*) (C:1*d*;H:1*p*), and diffuse functions (*D*) (C:1*d*;H:1*p*). In some calculations we replaced the (*D*) functions by "Rydberg" functions (*R*) expanded at the center of symmetry. These are diffuse GTO functions with exponents obtained by calculating the maximal overlap with the hydrogenic orbital for each chosen *nl* quantum number. Functions for 3*s*, 4*s*, 3*p*, 4*p* in the Rydberg series were obtained this way.

All results presented in this work have been obtained with the SIRIUS/ABACUS program package for multiconfiguration self-consistent field (MCSCF) wavefunctions, linear and quadratic response functions [44, 45, 25, 6] and geometry related properties [46]. The phosphorescence yields use the multiconfiguration quadratic response (MCQR) theory formulation for singlet and triplet operators by Vahtras et al. [6]. One- and two-electron electrostatic and spin–orbit integrals were obtained over generally contracted gaussian type orbitals (GTO:s) by means of the HERMIT program [47], which is interfaced to SIRIUS. The spin–orbit integrals are full two-center integrals containing both one- and two-electron components [5].

The MCQR program is implemented for complete (CAS) and restricted active space (RAS) functions. In the present work we employ complete active spaces of π orbitals correlating all π electrons. We base the use of these active spaces on occupation number criteria from MP2 and MCSCF calculations, see also [7, 48]. As seen in Table 2 with these active spaces the linear response excitation energies agree with the (recently revised) experimental energies within two tenths of an eV. A recent calculation by Roos et al. [49] using the CASPT2 method indeed indicated minor changes in energy for the $^3B_{1u}$ and $^3E_{1u}$ states – only some hundredths of an eV – when applying a perturbation theory expansion on the CAS Π space wavefunctions ($^3A_{2u}$ was not included). The geometry of the regular hexagonal benzene molecule is 1.339 Å for the C–C and 1.101 Å for the C–H bond. The caption to Table 2 gives the active space orbitals in D_{6h} notation.

3.2.2 MCQR results for the $^3E_{1u}$ and $^3A_{2u}$ radiative decay and a crude vibronic estimation of the benzene phosphorescence lifetime. In this section we first consider the MCQR calculations of phosphorescence transition moments without considerations of vibronic coupling. This means that we calculate the interactions leading to the decay of the $^3E_{1u}$ and $^3A_{2u}$ states, excluding the vibronic interactions in the four different mechanisms depicted in Fig. 1. The final transition moments and the lifetimes for the $^3B_{1u}$ state presented here as "*ab initio*" are in this section obtained from a combination of MCQR phosphorescence moments and CNDO/S-CI vibronic coupling constants described in the previous section. The description of the direct *ab initio* calculations of the vibronic phosphorescence for the $^3B_{1u} \rightarrow {}^1A_{1g}$ intensity is deferred to the next section.

Table 2. The ground and triplet state energies (eV) calculated with RPA and MCLR for double (DZ), triple (TZ), triple polarized (TZP) zeta basis set and with diffuse (*D*) or "Rydberg" (*R*) functions for states relevant for phosphorescence in benzene. Oscillator strengths (f_l, length, and f_v, velocity) are shown for the $^1E_{1u}$ state. The TRK-sums for the different components are shown in the rightmost column. The MCQR results are obtained for different Π CAS spaces as explained below

Level	g.s. energy (a.u.)	Triplet states			Singlet states		$^1E_{1u}$		TRK-sum	
		$^3B_{1u}$	$^3E_{1u}$	$^3A_{2u}$	$^1A_{2u}$	$^1E_{1u}$	f_l	f_v	$S(0)_{x,y}$	$S(0)_z$
Expt		3.66[b]	4.54[c]	6.93[d]	6.93[b]	7.59[e]				
CNDO/S-CI		2.95	4.07	6.39	6.39	7.10				
DZ-RPA	−230.6382	[a]	4.94	9.05	9.49	7.82	1.578	1.136	–	–
DZ-CAS(ΠA)	−230.7197	3.38	4.88	9.41	9.69	8.35	1.418	0.972	2.89	1.88
DZ-CAS(ΠC)	−230.7255	3.46	4.89	9.42	9.69	8.20	1.432	0.966	2.90	1.87
DZR-CAS(ΠB)	−230.7255	3.45	4.90	7.25	7.28	8.19	1.360	0.930	2.91	2.09
TZ-CAS(ΠA)	−230.7504	3.32	4.84	8.85	9.07	8.21	1.352	0.954	3.01	3.19
TZR-CAS(ΠB)	−230.7558	3.39	4.86	7.25	7.28	8.06	1.256	0.884	3.02	3.19
TZP-RPA	−230.7182	[a]	4.68	6.91	7.05	7.37	1.424	1.470	–	–
						8.00	0.011	0.016		
TZP-CAS(ΠA)	−230.7964	3.30	4.69	7.13	7.22	7.71	1.288	1.328	5.88	5.94
						8.93	0.010	0.006		
TZP-CAS(ΠD)	−230.8125	3.49	4.73	7.18	7.25	7.50	1.266	1.288	5.87	5.93
						8.04	0.070	0.080		
TZPR-CAS(ΠB)	−230.8068	3.43	4.71	7.10	7.16	7.24	0.406	0.402	5.88	5.94
						7.58	0.912	0.958		
						8.33	0.001	0.002		
TZPD-CAS(ΠA)	−230.8239	3.30	4.67	7.07	7.16	7.65	1.278	1.284	5.94	5.93
						8.63	0.044	0.050		

[a] Triplet instabilities
[b] Ref. [50]
[c] Ref. [57]
[d] Ref. [61]
[e] Ref. [49]
CAS-spaces:
$\Pi A = 1a_{2u}, 1e_{2u}, 1b_{2g}, 1-2e_{1g}$
$\Pi B = 1-3a_{2u}, 1e_{2u}, 1b_{2g}, 1-3e_{1g}$
$\Pi C = 1-3a_{2u}, 1-2e_{2u}, 1-2b_{2g}, 1-2e_{1g}$
$\Pi D = 1-3a_{2u}, 1-2e_{2u}, 1-2b_{2g}, 1-3e_{1g}, 1b_{1g}$

The quality of phosphorescence transition moments and lifetimes link indirectly to the quality of transition energies. In Table 2 we therefore list transition energies for the lowest triplet and singlet states as obtained from RPA and MCLR using the different basis sets and active spaces described in the previous section. We then only consider states that by symmetry are relevant for the phosphorescence problem in benzene. From Table 2 we see that the energy of the lowest $^3B_{1u}$ state is comparatively insensitive to basis sets and correlation spaces. Our best predicted value is 3.49 eV, less than 0.2 eV below the experimentally given value [50]. We note that there are two sets of experimental values referred to in the literature, in Refs. [12, 50] and [51], see also footnotes to Table 2. We note that both DZP-RPA and TZP-RPA suffer from triplet instabilities in that the first $^3B_{1u}$ state is obtained at very high energy. Such problems are well known in RPA calculations of triplet states [27]. The $^3E_{1u}$ excitation energy is also remarkably stable with respect to basis set and active space, giving variations in the order of 0.1 and 0.2 eV.

Both the $^3B_{1u}$ and the $^3E_{1u}$ states have dominant covalent character and are as such well described also by state-specific CASSCF calculations, as discussed in [7]. The excitation energy to the $\sigma\pi^*$ triplet state $^3A_{2u}$ is somewhat more dependent on basis set, especially in the inclusion of polarizing functions, the deviation is again within 0.2 eV from experiment.

Since radiative dipole interaction constitutes one leg of phosphorescence we report also singlet state transition energies and oscillator strengths in Table 2. Among the manifold of singlet states only those of $^1E_{1u}$ and $^1A_{2u}$ symmetries are relevant for the benzene phosphorescence problem. For these we obtain a somewhat larger basis set and active space dependency than for the triplets, for instance polarization functions are crucial. The 1^1E_{1u} state has particular interest, being the main carrier of the oscillator strength in the dipole spectrum. It has some ionic character, which has posed particular problems in state-specific calculations. As argued in [7, 49] the ionic character introduces polarization in the σ skeleton described by a dynamical σ–π correlation. The 1^1E_{1u} state also contains components of diffuse character, and obtains contributions from a Rydberg orbital close in energy. Roos et al. [49] note that in state-specific CASPT2 calculations the interfering Rydberg orbital should be included in the active space, and they assign the two experimental states at 6.94 and 7.59 eV to two $^1E_{1u}$ states, with valence and Rydberg character, respectively. It is thus interesting to note that with larger basis sets and active spaces MCLR calculations repeat the doubling of the $^1E_{1u}$ state in this energy region.

Table 2 also gives sums of oscillator strengths for individual transitions pertaining to singlet spectra in dipole length and velocity gauges. The $S(0)$-sum rule (Thomas–Reiche–Kuhn) indicates that the sum of oscillator strengths is equal to the number of active electrons (6). The equality between the parallel and perpendicular components, referring to the number of excitations in the two directions, provides another measure of completeness. We find a rather large deviation for the smallest basis set employed, DZ, but a deviation of only 0.1 electrons from the sum rule for the largest basis sets. Gauge invariance is within a few % for these basis sets.

Tables 3, 4 and 5 list the phosphorescence transition moments referring to the different mechanisms. In these tables the first column gives the energy of the triplet states which have vibrationless T–S_0 transition activity, the second column describes the pure spin–orbit induced electric dipole transition moments from MCQR computations, in the third column the "pure" transition moments are weighted with the vibronic coupling elements obtained from CNDO/S-CI, see Sect. 2. The fourth column gives the final oscillator strengths of the phosphorescent $^3B_{1u} \rightarrow {}^1A_{1g}$ transition [52].

For mechanism I + II one finds that the dipole transitions are weak but that the SOC is comparatively large, see Table 1 for comparison. In the case of mechanism III and IV the 1^1E_{1u} state plays an important role for the intensity borrowing, because of its huge dipole oscillator strength. For mechanism III the total phosphorescence yield is still small because of a small SOC (as studied by Clementi [16]). For mechanism IV CNDO/S-CI a fairly small SOC was predicted. However, for this mechanism MCQR predicts a quite different value. We see from Table 5 that the DZ-RPA and CNDO values are quite close, but along with improvement in wavefunction, the transition moment is increased by an order of magnitude. The splitting of the $^1E_{1u}$ states into one valence and one Rydberg component means that SOC occurs to more than one $^1E_{1u}$ state. Our results indicate that the total SOC interaction, remains about the same anyway. The

Table 3. Excitation energies of $^3E_{1u}$ state (eV) and transition moments (a.u.) and oscillator strengths for the $^3B_{1u}$–^1A_g transition with different basis sets and correlation levels, referring to phosphorescence mechanisms I and II with e_{2g} vibronic coupling (see caption to Table 1)

Level	Excitation energy	Transition moment		Osc. strength
	$^3E_{1u}$	$\langle ^3E_{1u}\|z\|^1A_{1g}\rangle$ M^z	$\langle ^3B_{1u}\|z\|^1A_{1g}\rangle$ M^z	$f_{10}^{x,y}$
CNDO/S-CI	4.07	$1.30e-4$	$4.9e-5$	$2.15e-10$
DZ-RPA	4.94	$1.81e-4$	$6.79e-5$	$4.13e-10$
DZ-CAS(ΠA)	4.88	$1.75e-4$	$6.56e-5$	$3.86e-10$
DZ-CAS(ΠC)	4.89	$1.73e-4$	$6.49e-5$	$3.78e-10$
DZR-CAS(ΠB)	4.90	$1.35e-4$	$5.06e-5$	$2.30e-10$
TZ-CAS(ΠA)	4.84	$9.10e-5$	$3.41e-5$	$1.04e-10$
TZR-CAS(ΠB)	4.86	$5.92e-5$	$2.22e-5$	$0.44e-10$
TZP-RPA	4.68	$3.91e-5$	$1.47e-5$	$0.19e-10$
TZP-CAS(ΠA)	4.69	$4.32e-5$	$1.62e-5$	$0.24e-10$
TZP-CAS(ΠD)	4.73	$2.63e-5$	$0.99e-5$	$0.09e-10$
TZPR-CAS(ΠB)*	4.71	$1.99e-5$	$0.75e-5$	$0.50e-11$

* Obtained from calculation using one-el. part of the H_{SO} and by multiplying the transition moment by the empirical factor of 1.7

Table 4. Excitation energies (eV) of $^3E_{1u}$ state, transition moments (a.u.) and oscillator strengths for the $^3B_{1u}$–$^1A_{1g}$ transition with different basis sets and correlation levels, referring to phosphorescence mechanism III with e_{2g} vibronic coupling (see caption to Table 1)

Level	Excitation energy	Transition moment		Osc. strength
	$^3E_{1u}$	$\langle ^3E_{1u}\|x(y)\|^1A_{1g}\rangle$ $M^{x,y}$	$\langle ^3B_{1u}\|x(y)\|^1A_{1g}\rangle$ $M^{x,y}$	f_{10}^{z}
CNDO/S-CI	4.07	$5.00e-5$	$1.88e-5$	$6.30e-11$
DZ-RPA	4.94	$7.58e-6$	$2.84e-6$	$1.45e-12$
DZ-CAS(ΠA)	4.88	$2.81e-6$	$1.05e-6$	$1.98e-13$
DZ-CAS(ΠC)	4.89	$3.27e-6$	$1.23e-6$	$2.71e-13$
DZR-CAS(ΠB)	4.90	$3.11e-6$	$1.17e-6$	$2.45e-13$
TZ-CAS(ΠA)	4.84	$9.11e-7$	$3.41e-7$	$2.08e-15$
TZR-CAS(ΠB)	4.84	$1.60e-6$	$6.00e-7$	$6.45e-14$
TZP-RPA	4.68	$3.84e-6$	$1.44e-6$	$3.72e-13$
TZP-CAS(ΠA)	4.69	$5.25e-6$	$1.97e-6$	$6.96e-13$
TZP-CAS(ΠD)	4.73	$5.47e-6$	$2.05e-6$	$7.53e-13$
TZPR-CAS(ΠB)*	4.71	$0.80e-5$	$0.30e-5$	$1.61e-12$

* See Table 3

consideration of SOC to only the lowest $^1E_{1u}$ state, however, is not enough, and might be one reason for the low SOC and small role of mechanism IV obtained from the semi-empirical calculations as compared to MCQR. A considerable increase in the SOC between $^3A_{2u}$ and $^1E_{1u}$ is obtained going from small to large wavefunctions, with the CNDO/S-CI results comparing with the former. Furthermore, the spin–orbit interacting $^3A_{2u}$ and the first $^1E_{1u}$ states are very close in

Table 5. Excitation energies of $^3E_{1u}$ state (eV), transition moments (a.u.) and oscillator strengths for the $^3B_{1u}$–$^1A_{1g}$ transition with different basis sets and correlation levels, referring to phosphorescence mechanism IV with b_{2g} vibronic coupling (see caption to Table 1)

Level	Excitation energy	Transition moment		Osc. strength
	$^3A_{2u}$	$\langle ^3A_{2u}\|x(y)\|^1A_{1g}\rangle$ $M^{x,y}$	$\langle ^3B_{1u}\|x(y)\|^1A_{1g}\rangle$ $M^{x,y}$	$f_{10}^{x,y}$
CNDO/S-CI	6.39	$2.00e-4$	$1.40e-5$	$1.76e-11$
DZ-RPA	9.05	$1.26e-4$	$8.82e-6$	$6.97e-12$
DZ-CAS(ΠA)	9.41	$8.14e-5$	$5.70e-6$	$2.91e-12$
DZ-CAS(ΠC)	9.42	$9.17e-5$	$6.42e-6$	$3.69e-12$
DZR-CAS(ΠB)	7.25	$5.95e-4$	$2.23e-5$	$4.46e-11$
TZ-CAS(ΠA)	8.85	$8.47e-4$	$3.18e-5$	$9.06e-11$
TZR-CAS(ΠB)	7.25	$8.20e-4$	$3.08e-5$	$8.50e-11$
TZP-RPA	6.91	$1.26e-3$	$8.82e-5$	$6.97e-10$
TZP-CAS(ΠA)	7.13	$1.02e-3$	$7.14e-5$	$4.57e-10$
TZP-CAS(ΠD)	7.18	$1.55e-3$	$1.10e-4$	$10.8e-10$
TZPR-CAS(ΠB)*	7.10	$1.49e-3$	$1.05e-4$	$9.8e-10$

* See Table 3

energy and an accurate description of both is essential. One should also add the contribution from the full manifold of $^3E_{1u}$ states, as accounted for by MCQR.

There are clear trends in the dependence of transition moments on improvements of the basis sets and correlation of the ground-state wavefunction. Concerning the different mechanisms our results give the following predictions: For mechanisms I and II the transition moment is fairly large for the DZ basis set, but decreases when we apply larger basis sets and correlation spaces. The results at the DZ level are close to CNDO/S-CI but deviate for larger basis sets. For mechanism III we have the opposite trend meaning that the in-plane polarization transition moment increases with better basis set. Mechanism IV is also in-plane-polarized with the transition moment increasing with the basis set and accuracy of the wavefunction. This means that we have an "inflection point" in the relative importance of the various mechanisms; for small wavefunctions mechanisms I and II dominate over mechanism IV, while the reverse holds at large wavefunctions. Mechanism III shows larger fluctuation with wavefunctions, but remains negligible with respect to I, II and III for all entries.

It is of interest to note that both mechanisms III and IV involve spin–orbit coupling to and phosphorescence through the $^1E_{1u}$ state. This state, with its ionic character and diffuse components, requires a high-level calculation, as previously noted in optimization of its total energy [49]. We also find this state to be associated with a satellite, with probable Rydberg character. In calculations using small basis sets (n.b. DZ basis sets) we obtain results rather close to those of CNDO/S-CI, while results deviate for larger basis sets, mostly due to mechanism IV. The radiative lifetime obained with spin and dipole interactions treated *ab initio* and vibronic interaction semi-empirically lies in the region 2–10 s (Table 6), which is too low in comparison with direct vibronic phosphorescence calculations, see next section (actually it fits better with the total lifetimes observed by Rabalais et al. [53]). This is linked to an overestimated intensity ratio between e_{2g} (mechanism I + II) and b_{2g} (mechanism IV) bands [12], and hence a more intensive in-plane

Table 6. Lifetimes τ (s) of the $^3B_{1u}$ state for different basis sets and correlation levels (see caption to Table 1) referring to the four different mechanisms. τ_{av} refers to the average of the $\tau_{x,y}^{Tot}$ and the τ_z^{III} lifetimes

Level	$\tau_{x,y}^{I+III}$	$\tau_{x,y}^{IV}$	$\tau_{x,y}^{Tot}$	τ_z^{III}	τ_{av}
CNDO/S-CI	7.99	97.7	7.39	27.3	9.76
DZ-RPA	4.17	246.8	4.10	1186	6.14
DZ-CAS(ΠA)	4.46	591	4.43	8688	6.64
DZ-CAS(ΠC)	4.55	466	4.51	6348	6.76
DZR-CAS(ΠB)	7.48	38.6	6.27	7010	9.40
TZ-CAS(ΠA)	16.5	19.0	8.83	82701	13.2
TZR-CAS(ΠB)	39.1	20.2	13.3	26654	19.9
TZP-RPA	90.5	2.47	2.40	4624	3.60
TZP-CAS(ΠA)	71.7	3.76	3.57	2472	5.35
TZP-CAS(ΠD)	191	1.59	1.58	2284	2.37
TZPR-CAS(ΠB)*	344	1.76	1.75	1068	2.62

polarization than observed [10, 54]. The reason for this deviation seems to be connected with that the CNDO method overestimates the vibronic interaction between the 1^3B_{1u} and the 1^3A_{2u} states.

As in the case of benzene fluorescence, the $^1E_{1u}$ state, which strongly dipole interacts with the ground state, seems to be the important entity in the phosphorescence case. The description of the SOC between $^3E_{1u}$ and $^1E_{1u}$ and between $^3A_{2u}$ and $^1E_{1u}$, is thus crucial, the latter two states being nearly degenerate in energy. The spin–orbit coupling is obtained as weak in the former but strong in the latter case. These facts indicate the importance of handling the full form of the spin–orbit interaction, and to treat more than the lowest states of each symmetry. The previous semi-empirical calculations, as well as previous *ab initio* approaches to phosphorescence, see e.g. [54, 55, 56], handle this problem by truncated and often slowly convergent sum-over-state procedures, while the quadratic response functions implicitly contain all contributions.

It should be born in mind that all lifetime entries in Table 6 are obtained here with the semi-empirically determined vibronic factors $H(e_{2g})$ and $H(b_{2g})$. In the lifetime determination we also have a crucial E^3-factor, where E is the excitation energy of the $^3B_{1u}$ state. The two experimental values reported are 3.66 [50] and 3.95 [51] eV, the choice between them is crucial (we choose the former, closest to the MCLR results presented here, for the lifetime entries in Table 6). The CNDO/S-CI energy of 2.95 eV leads to a lifetime of 15.4 sec, however, with an excitation energy of 3.66 eV this value halves (see Table 6).

4 Direct *ab initio* calculation of the vibronic phosphorescence $^3B_{1u} \rightarrow {}^1A_{1u}$ intensity by the MCQR approach

In order to solve the benzene phosphorescence problem completely *ab initio*, we have obtained the T_1–S_0 transition moments of Eq. (37) for few vibrational modes by direct MCQR calculations of the derivatives of Eq. (39). In the latter equation the numbers n and 0 then correspond to the states 1^3B_{1u} and 1^1A_{1g}, respectively. The force field, vibrational normal modes and frequencies have been obtained with the ΠA active space (see Table 2) and with the DZ basis set. The calculated and

Table 7. Comparison between experimental and calculated vibrational frequencies (in cm^{-1}) for the e_{2g} and b_{2g} vibrational modes

Wilson notation		ν_{Exp}	ν_{Cal}
e_{2g}	ν_8	1601	1726
	ν_6	606	662
	ν_9	1178	1293
	ν_7	3057	3374
b_{2g}	ν_4	703	738

observed frequencies of the e_{2g} and b_{2g} modes, which are relevant for the benzene phosphorescence problem are represented in Table 6. The most important vibrations (ν_4, ν_6, ν_7, ν_8 and ν_9) from the CNDO/S-CI treatment have been included in MCQR calculations of the vibronic phosphorescence intensities. The T_1–S_0 transition dipole moments have been calculated by the MCQR method using distorted benzene geometries with atomic displacements along the normal modes. We would like to stress that the quadratic response technique is particularly useful for such kind of direct calculations, because all contributions to the sum of Eq. (2) are accounted for completely. In ordinary perturbation theory the truncation of the row of Eq. (2) at distorted geometry along a vibrational mode produces a serious size-consistency problem for the vibronic intensity [31]. The derivatives of Eq. (39) have been obtained by numerical differentiation. Calculated transition moments from Eq. (37) for the different vibronic modes $^3B_{1u}(v = 0) \rightarrow {}^1A_{1g}(v = 1)$ are represented in Table 7. A number of active spaces and basis sets have been checked in these calculations. The lowering of symmetry in the vibrational movement introduces some limitations of basis sets and the use of electronic correlation. The e_{2g} vibronic band ($\nu_8 = 1601$ cm^{-1}) appears to be the most intensive one. The out-of-plane b_{2g} vibration is very sensitive to the choice of active space and produces few broken symmetry results depending on the extension of σ–π correlation, which cannot be excluded in this case. This σ–π-correlation includes the $3e_{2g}$ occupied σ-orbitals and the $4e_{1u}$ unoccupied σ^*-orbitals. A proper indication of a well-balanced active space solution for the b_{2g} distortion geometry is that the transition moment of the x and y components are equilibrated. For other non-equilibrated results obscure high-transition moments occur for the z-polarized transition moment. Finally, we have obtained the proper polarized transition moments for the vibronic ν_4 phosphorescence from the $^3B_{1u}^{x,y}$ spin-sublevels. Its intensity is an order of magnitude smaller than that for the ν_8 transition, see Table 7, in good agreement with observations [12].

5 Discussion

In the preceding we have described first the results from calculations of singlet–triplet vertical transitions intensities involving 1^3A_{2u}, 1^3E_{1u} and 1^3B_{1u} upper states. All results are connected with the singlet ground state optimized geometry and for the last state they also account for the ground state vibrations. In relevance with $T_n \leftarrow S_0$ absorption measurements [58] and with the historical account of the benzene phosphorescence problem [36, 37] we can conclude from

the most extensive active space TZPR-CAS (ΠB) calculations that the 1^3A_{2u}–$^1A_{1g}$ transition in the UV region (7.1 eV, Table 5) has the largest predicted intensity ($M_{x,y} = 0.0015$ a.u. and $f(T \leftarrow S_0) = 2.8 \times 10^{-6}$). Here and throughout the paper the lower sign denotes an electric dipole polarization and the upper sign denotes a spin-sublevel symmetry. The $^3E_{1u} \leftarrow {}^1A_{1g}$ absorption has much smaller intensity ($M_{x,y} = 8{\cdot}10^{-6}$ a.u., Table 4; $M_z = 2{\cdot}10^{-5}$ a.u., Table 3, and the total $f = 2.18{\cdot}10^{-10}$) which is mainly (76%) out-of-plane polarized. In accordance with the simple CNDO/S-CI vibronic mixing calculations of Eqs. (28)–(34), (52) and (57) this intensity is borrowed from the $^3B_{1u}$–$^1A_{1g}$ transition. It leads to a very large intensity of the b_{2g} vibrational mode ν_4 in the phosphorescence spectrum (mechanism IV, $f^{x,y} = 10^{-9}$) in comparison with the e_{2g} modes (mechanisms I, II and III, Tables 3 and 4; the total $f \simeq 10^{-10}$). It forces us to suspect that the out-of-plane b_{2g} vibrational mixing of Eq. (57) is highly overestimated in CNDO/S-CI approximation in comparison with the mixing of Eq. (52), induced by in-plane e_{2g} modes.

Much more reliable results have been obtained by the direct *ab initio* calculations of the $^3B_{1u} \rightarrow {}^1A_{1g}$ phosphorescence vibronic transition intensities (Table 7). The most intensive e_{2g} vibronic band ν_8 appears to be predominantly out-of-plane polarized (mechanism I + II) with the f value of the order 10^{-10} for all basis sets; the values of DZ-quality are slightly higher than the TZ results. From the most reliable TZR(ΠB) results the phosphorescence emission in this band from each (x and y) spin-sublevel is characterized by the electric dipole transition moment equal to 1.62×10^{-5} a.u. This corresponds to the oscillator strength for the absorption in this "hot" band equal to 0.42×10^{-10} and to the radiative lifetime of 15 sec (In the latter case we must take into account the degeneracy of the e_{2g} vibration). The in-plane polarization of this band (mechanism III) is much weaker; the intensity ratio for the out-of-plane to the in-plane polarized $e_{2g}(\nu_8)$ vibronic phosphorescence emission is equal to 200 in the TZR-basis set and is even larger for the smaller basis sets. Quite similar results are obtained for the next e_{2g} C–C stretching mode $\nu_9 = 1178\ \mathrm{cm}^{-1}$, besides the fact that it has approximately two times smaller intensity. The ν_8/ν_9 intensity ratio is equal to 2.03, 2.18 and 2.36 in TZR, DZR and DZ basis sets, respectively. The out-of-plane polarization of the ν_9 band dominates completely (Table 8). The other vibronic band ($\nu_6 = 606\ \mathrm{cm}^{-1}$) of the same symmetry is not highly polarized, but its intensity is approximately three orders of magnitude smaller than that of the ν_8 band. In DZ- and TZ-basis sets this ratio is equal to 0.0045 and in DZR- and TZR-basis sets it is approximately 0.002. Obviously the account of Rydberg orbitals diminishes the ratio of ν_6/ν_8 vibronic intensities. The calculated intensity of ν_7 (3057 cm^{-1}) e_{2g} vibronic band is also negligible in comparison with strong ν_8, ν_9 phosphorescence transitions which is in accordance with observations.

The microwave induced delayed phosphorescence (MIDP) experiments [54] for a C_6H_6/C_6D_6 doped crystal at 4.2 K shows that ν_6 vibronic transitions from the z triplet spin-sublevel also have some nonvanishing activity. This is in a good agreement with our TZR result (Table 7), where the z spin-sublevel has a larger intensity than the x, y sublevels for the ν_6 mode. It means that the different modes of the same e_{2g} symmetry (the C–C stretching vibrations ν_8, ν_9 and the skeletal in-plane bending ν_6 vibration) produce different types of SOC perturbations on the x, y and z spin-sublevels in complete agreement with MIDP observations [54].

The b_{2g} vibronic phosphorescence band has smaller intensity, in comparison with the $e_{2g}(\nu_8$ and $\nu_9)$ emission, but nevertheless it might be observable under the typically old conditions for recording of phosphorescence spectra [12, 17, 10]. We consider this as a serious achievement of MCQR theory. The b_{2g} vibronic

Table 8. Transition moments calculated with direct vibronic coupling. Excitation energies (eV), transition moments (a.u.) for the different mechanisms performed for different basis sets and correlation levels (see caption to Table 1)

Level			Excitation energy	Transition moment M	Osc. strength f_i	Σf_i
	Mechanisms I + II			$\lvert\langle {}^3B_{1u}^{x,y}\rvert z\rvert {}^1A_{1g}\rangle\rvert$		
e_{2g}	ν_8(1601)	DZ(ΠB)	3.34	$2.86e-5$	$0.733e-10$	
	ν_9(1178)		3.38	$1.86e-5$	$0.310e-10$	
	ν_6(606)		3.38	$1.90e-6$	$0.003e-10$	
	ν_7(3057)		3.38	$1.49e-6$	$0.002e-10$	
						$1.05e-10$
	ν_8(1601)	DZR(ΠB)	3.34	$2.41e-5$	$0.521e-10$	
	ν_9(1178)		3.38	$1.63e-5$	$0.238e-10$	
	ν_6(606)		3.39	$9.91e-7$	$0.001e-10$	
	ν_7(3057)		3.39	$2.04e-6$	$0.004e-10$	
						$0.76e-10$
	ν_8(1601)	TZ(ΠB)	3.28	$1.27e-5$	$0.145e-10$	
	ν_9(1178)		3.32	$9.81e-6$	$0.086e-10$	
	ν_6(606)		3.33	$6.27e-7$	$0.004e-11$	
	ν_7(3057)		3.33	$5.26e-7$	$0.003e-11$	
						$0.23e-10$
	ν_8(1601)	TZR(ΠB)	3.29	$1.62e-5$	$0.235e-10$	
	ν_9(1178)		3.32	$1.22e-5$	$0.133e-11$	
	ν_6(606)		3.33	$1.27e-7$	$0.001e-12$	
	ν_7(3057)		3.33	$5.94e-7$	$0.003e-11$	
						$0.37e-10$
	Mechanism III			$\lvert\langle {}^3B_{1u}^{x}\rvert x(y)\rvert {}^1A_{1g}\rangle\rvert$		
e_{2g}	ν_8(1601)	DZ(ΠB)	3.34	$1.48e-6$	$0.393e-12$	
	ν_9(1178)		3.38	$1.86e-7$	$0.006e-12$	
	ν_6(606)		3.38	$1.64e-7$	$0.004e-12$	
	ν_7(3057)		3.38	$1.53e-8$	$0.004e-14$	
						$0.40e-12$
	ν_8(1601)	DZR(ΠB)	3.34	$1.46e-6$	$0.382e-12$	
	ν_9(1178)		3.38	$5.95e-7$	$0.063e-12$	
	ν_6(606)		3.39	$2.11e-7$	$0.008e-12$	
	ν_7(3057)		3.39	$9.48e-8$	$0.002e-12$	
						$0.46e-12$
	ν_8(1601)	TZ(ΠB)	3.28	$1.15e-6$	$0.237e-12$	
	ν_9(1178)		3.32	$3.65e-7$	$0.012e-12$	
	ν_6(606)		3.33	$4.07e-7$	$0.030e-12$	
	ν_7(3057)		3.33	$1.80e-7$	$0.006e-12$	
						$0.29e-12$
	ν_8(1601)	TZR(ΠB)	3.29	$1.14e-6$	$0.233e-12$	
	ν_9(1178)		3.32	$3.54e-7$	$0.022e-12$	
	ν_6(606)		3.33	$4.15e-7$	$0.031e-12$	
	ν_7(3057)		3.33	$1.93e-7$	$0.007e-12$	
						$0.29e-12$

Table 9. Transition moments calculated with direct vibronic coupling. Excitation energies (eV), transition moments (a.u.) for the mechanisms obtained for different basis sets and with correlation levels Π, which includes the 3 highest occupied and 3 lowest unoccupied π-orbitals, and $\Sigma\Pi$, which except the Π-orbitals also includes the 2 highest occupied and 2 lowest unoccupied σ-orbitals

Level			Excitation energy	Transition moment M	Osc. strength
	Mechanisms IV			$\lvert\langle {}^3B_{1u}^{x,y}\rvert x(y)\rvert {}^1A_{1g}\rangle\rvert$	
b_{2g}	$\nu_4(707)$	DZ(Π)	3.27	$6.23e-6$	$0.35e-11$
	$\nu_4(707)$	DZR(Π)	3.27	$5.84e-6$	$0.31e-11$
	$\nu_4(707)$	TZ($\Sigma\Pi$)	3.31	$3.38e-6$	$0.10e-11$
	$\nu_4(707)$	TZR($\Sigma\Pi$)	3.31	$3.16e-6$	$0.09e-11$

transition from the x spin–sublevel has y-polarization and vice versa. The calculated ν_8/ν_4 intensity ratio in DZ-, DZR- and TZ-basis sets is equal to 20.9, 16.8 and 14.5, respectively. In the observed phosphorescence spectrum the very weak b_{2g} intensity shows signs of predominantly in-plane polarization [10] which completely corresponds to our direct MCQR calculation. The typical intensity distribution among all calculated vibronic bands ($\nu_8:\nu_9:\nu_6:\nu_7:\nu_4$) in benzene phosphorescence spectrum are as follows (DZ-basis set): 67.6%: 28.6%: 0.3%: 0.2%: 3.2%. Approximately 98% of the phosphorescence intensity has out-of-plane polarization. This is in accordance with the MIDP experimental findings [54]: van Egmond and van der Waals have pointed out that the earlier polarization measurements [10] at 77 K could not exclude some molecular rotation in the glass and 70% polarization is therefore an underestimation. In the low temperature (4.2 K) MIDP experiments more than 90% out-of-plane polarized phosphorescence has been recorded [54].

The combination of the Zeeman and MIDP techniques on the most intensive (8_1^0) vibronic phosphorescence band definitely shows that the radiative rate constants (k) for x and y spin-sublevels are equal to each other (k_z being negligible) and fit to the relation $k_x = k_y = 0.15\ s^{-1}$. In simulation of the MIDP spectra it was found that if such a system starts to decay with a Boltzman distribution over the spin-sublevels corresponding to a temperature of 1.3 K then the decay will be very nearly exponential with the observed lifetime of 10 s and after the experimental delay time the sublevels population distribution $N_x:N_y:N_z$ will be very close to the observable ratio 72:76:100 [54]. This feature is in a good agreement with calculated radiative rate constants of the ν_8 band. In the DZ basis set we have for this band $k_x = k_y = 0.042\ s^{-1}$ and $k_z = 0.0001\ s^{-1}$; the averaged lifetime is 23.5 s. Besides ν_8, the largest contribution to the total radiative lifetime is given by the ν_9 band. The total phosphorescence radiative lifetimes calculated in different basis sets are 24 (DZ), 33 (DZR), 107 (TZ) and 68 (TZR) seconds.

Experimental data are given with solvated benzene or with benzene isolated on matrices, while data on benzene vapour are missing. Measured total lifetimes are also dependent on non-radiative decay channels. These channels are activated mostly by spin–vibronic interactions between the triplet and the ground states and are known, for other compounds, to be extremely dependent on perturbations due to geometric conformation, on isotope substitution and on solvent interactions.

The lifetime measured for benzene in solution favour lower values than theoretically predicted for the radiative part; Wright et al. [59] predicted the lifetime of $C_6H_6(C_6D_6)$ in solid (at 4.2 K) CH_4, Ar, Kr, and Xe to 16 (22), 16 (26), 1 (1), 0.07 (0.07) sec, respectively. This series of observations is a nice confirmation of that both vibronic and spin–orbit coupling is involved in the phosphorescence process in benzene: The contribution of vibronic coupling is evidenced by that deuteration leads to longer lifetimes; the spin–orbit coupling by the drastic shortening of lifetime (increase of yields) in the presence of an heavy atom ("the heavy atom effect" [50]). Colson [60] obtains the lifetime of deuterated benzene in different "isotropic traps" in the region of 8 to 9 sec; Rabalais et al. [53] report mean phosphorescence lifetimes of benzene in various glassy solvents in the range between 3 and 8 sec. They make the interesting observation that the lifetime is decreased with the polarity of the solvent. They confirm the increase of benzene lifetime with deuteration (roughly a factor 1.5 between C_6H_6 and C_6D_6), and state this as one example of a general trend for hydrocarbons. Because the deuteration diminishes the non-radiative decay of the T_1 state in hydrocarbons [50] the lifetime of C_6D_6 in solid argon must be a lower limit to the radiative phosphorescence lifetime τ_r of benzene. The "best experimental" value for the intrinsic (or radiative) lifetimes is $\simeq 30$ s [53].

6 Conclusions

The radiative lifetime of triplet benzene still poses a considerable challenge for quantum chemistry. This is reflected by the quite different results and interpretations presented by previous semi-empirical calculations [10, 15, 16, 32, 53] and also by the information obtained from different experiment techniques which not always have been consistent neither with respect to the total lifetime nor the polarization of emission. We now know that the phosphorescence radiation from the benzene molecule is the result of a number of involved interactions, simultaneously including dipole, spin–orbit and vibronic couplings acting in several channels. These interactions are in general weak, leading to a radiative lifetime much longer than that for triplet π–π^* states in heteroatomic aromatic compounds [50].

In the present work we have addressed the benzene phosphorescence problem at three levels of theory:

A. Semiempirical, CNDO/S-CI, calculations using Herzberg–Teller perturbation theory for the vibronic coupling.
B. *Ab initio* multiconfigurational response calculations using Herzberg–Teller perturbation theory for the vibronic coupling.
C. Direct *ab initio* multiconfigurational response calculations of vibronic phosphorescence.

These methods provide us with results of different accuracy concerning transition moments and lifetimes of benzene phosphorescence and different ways for interpreting experimental results as we will summarize below.

Methods A and B differ, apart from the usual semi-empirical approximations, in that **A** uses a truncated sum-over state procedure for the phosphorescence interaction, while the MCQR method sums all contributions. They both utilize the H–T perturbation theory for the vibronic interaction in which the radiative route is obtained via vibronic coupling between the $^3B_{1u}$ and the $^3A_{2u}$ and $^3E_{1u}$ states, the

latter phosphorescing to the ground state. This leads to the four phosphorescence mechanisms I–IV, depicted in Fig. 1. Our calculations using methods **A** and **B** contribute to the interpretation of benzene phosphorescence in the following way: The mechanisms depicted as I and II in Fig. 1 retain largely their strengths by the present calculations; mechanism III, cherished by the early studies, is attributed a decreased (negligible) importance, while mechanism IV, appears to be rather sensitive to the proper treatment of vibronic and spin–vibronic perturbations. In the Herzberg–Teller (H–T) perturbation theory the CNDO/S-CI method overestimates the vibronic mixing between $^3B_{1u}$ and $^3A_{2u}$ states, induced by out-of-plane b_{2g} ($\nu_4 = 707\ \mathrm{cm}^{-1}$) vibrations. On the other hand the $^3E_{1u}$–$^3B_{1u}$ vibronic mixings, induced by e_{2g} C–C stretching vibrations ($\nu_8 = 1601\ \mathrm{cm}^{-1}$ and $\nu_9 = 1178\ \mathrm{cm}^{-1}$) are underestimated in semiempirical treatments of the H–T expansion [10, 32, 53]. The combination of the H–T vibronic CNDO expansion with *ab initio* MCQR calculations of the $^3E_{1u}$ and $^3A_{2u}$ radiative to ground state transition intensities gives, in view of results with method **C** described below, an exaggerated b_{2g} activity, and therefore a too low benzene phosphorescence lifetime. The phosphorescence moments for the $^3A_{2u}$ and $^3E_{1u}$ states seems to converge with respect to the parametrization of the wavefunction, and the exaggeration is attributed to the CNDO computed vibronic constants. One additional reason is probably connected with that spin–vibronic interactions [10] are not account for in the H–T treatment of Eq. (40).

We noted that two of the mechanisms (III and IV) involve spin–orbit coupling to and phosphorescence through the $^1E_{1u}$ state, which is a notoriously "difficult" state due to its ionic character and diffuse components [49]. As in the case of benzene fluorescence it is thus also important for the phosphorescence case in the perturbative H–T treatment. In this connection the importance of handling the full form of the spin–orbit interaction was stressed, as well as the treatment of more than the lowest states of each symmetry and the account of all contributions in the sum-over-state expression as obtained with the quadratic response theory.

Method C removes the shortcomings of the restricted H–T approach in that the semiempirical pure-vibronic treatment has been replaced by direct *ab initio* MCQR calculations of the derivatives of the T_1–S_0 transition moment upon different normal modes. The complete sum-over-state implementation of the response approach removes the serious size-consistency problem for the vibronic intensity when using a truncated perturbation expansion along differently distorted geometries. We find that the e_{2g} C–C stretching modes ν_8 and ν_9 appear to be the most intensive vibronic phosphorescence bands with predominantly (92–98%) out-of-plane polarization in all basis sets. They share 65% and 32% of the total phosphorescence intensity in the largest TZR basis set, respectively, (69% and 29%, respectively, in the DZ basis and approximately the same ratios with other basis sets). In a very good accordance with observations [10, 12] the b_{2g} mode $\nu_4 = 707\ \mathrm{cm}^{-1}$ induces 3.5% of the total intensity (TZR). In other calculations it brings 1.4% (DZR, DZ) and 7.7% (TZ). It also origins from x, y spin-sublevels, but exhibits in-plane polarization in agreement with MIDP experiments [54]. The MIDP technique reveals that the very weak e_{2g} vibronic band ν_6 has comparable intensity for all three spin-sublevels in drastic difference with the other phosphorescence vibronic bands [54]. This fine feature is nicely reproduced in our calculations. Excluding the smallest (DZ) basis set, all others predict comparable intensities for x, y and z spin-sublevels and the TZ basis results reproduce the observed intensity ratio quite well.

We find that the lifetime of triplet benzene is the result of a delicate sum of contributions from several vibronic degenerate and non-degenerate modes. The direct vibronic phosphorescence calculations predict large values; the radiative lifetimes of $x(y)$ spin-sublevels are equal to 16, 22, 71 and 42 s in DZ, DZR, TZ and TZR basis sets, respectively (the z-sublevel lifetimes are of the order 4000–7000 s). For the high spin-lattice relaxation limit with an equilibrium spin population during the phosphorescence decay, the total radiative lifetimes are equal to 24, 33, 107 and 64 s in the respective basis sets. This trend seems to focus on a doubling of the accepted, but certainly not established, "best experimental value" of the intrinisic (or radiative) phosphorescence lifetime for the benzene molecule; $\simeq$ 30 s [53, 59]). Our best basis set value thus indicates that it takes a full minute for triplet benzene to depopulate through radiation.

Acknowledgements. We thank Poul Jørgensen for valuable discussions. This work was supported by grants from CRAY Research Inc. and the Swedish Institute (B.F.M.).

References

1. Parr RG, Craig DP, Ross IG (1950) J Chem Phys 18:1561
2. Fischer-Hjalmars I (1960) Sv Kemisk tidskr 72:612
3. Fischer-Hjalmars I (1962) Arkiv Fysik 21:123
4. Fischer-Hjalmars I, Sundbom M (1968) Acta Chem Scand 22:607
5. Vahtras O, Ågren H, Jørgensen P, Jensen HJA, Helgaker T, Olsen J (1992) J Chem Phys 96:2118
6. Vahtras O, Ågren H, Jørgensen P, Jensen HJA, Helgaker T, Olsen J (1992) J Chem Phys 97:9178
7. Matos JHO, Roos BO, Malmqvist PÅ (1987) J Chem Phys 86:1458
8. Fülscher MP, Andersson K, Roos BO (1992) J Phys Chem 96:9204
9. Fülscher MP, Malmqvist PÅ, Roos BO (1990) In: Lakowitz LR (ed) Time-resolved spectroscopy in biochemistry II, page 322. Proc SPIE
10. Albrecht AC (1963) J Chem Phys 38:354
11. Goeppert-Mayer M, Sklar AL (1938) J Chem Phys 6:645
12. Shull HJ (1949) J Chem Phys 17:295
13. McClure DS (1952) J Chem Phys 20:682
14. Sklar AL (1937) J Chem Phys 5:669
15. Mizushima M, Koide S (1952) J Chem Phys 20:765
16. Clementi E (1961) J Mol Spectroscopy 6:497
17. Dikun PP, Sveshnikov BY (1949) Zhur Eksptl i Teoret Fiz (Soviet JETP) 19:1000
18. Henry BR, Siebrand W (1969) J Chem Phys 51:2396
19. Krishna VG, Salzman WR (1969) J Chem Phys 50:3875
20. Olsen J, Jørgensen P (1985) J Chem Phys 82:3235
21. Breit G (1929) Phys Rev 34:553
22. Pauli W (1927) Z Phys 43:601
23. Thomas LT (1927) Phil Mag 3:1
24. Ågren H, Vahtras O (1993) J Phys B: At Mol Phys 26:913
25. Hettema H, Jensen HJA, Jørgensen P, Olsen J (1992) J Chem Phys 97:1174
26. Vahtras O, Ågren H, Jensen HJA, to be published.
27. Olsen J, Yeager DL, Jørgensen P (1991) Chem Phys Lett 186:379
28. Jensen HJA, Ågren H (1984) Chem Phys Lett 110:140
29. Siegbahn PEM, Heiberg A, Almlöf J, Roos BO (1981) J Chem Phys 74:2384
30. Olsen J, Roos BO, Jørgensen P, Jensen HJA (1989) J Chem Phys 89:2185
31. Mineav BF (1979) Fizika Molecul 7:34
32. Mineav BF (1971) Izv Vysch Uccheb Zeved Fizika 8:118
33. Roche M, Jaffé HH (1974) J Chem Phys 60:1193
34. Nishimoto K, Mataga N (1957) Z Physik Chem 12:335

35. Neto M, Scrocco M, Califano S (1961) Spectrochim Acta 22:1981
36. Hameka HF, Oosterhoff JL (1958) Mol Phys 1:364
37. Mizushima M, Koide S (1953) J Chem Phys 20:765
38. Veeman WS, Van der Waals JH (1970) Mol Phys 18:63
39. Knuts S, Vahtras O, Ågren H (1992) THEOCHEM 279:249
40. Ågren H, Vahtras O, Knuts S, to be published.
41. Dunning Jr TH (1970) J Chem Phys 53:2833
42. Dunning Jr TH (1971) J Chem Phys 55:716
43. Sadlej A (1988) Collection Czech Chem Commun 53:1995
44. Jensen HJA, Ågren H (1986) J Chem Phys 104:229
45. Jørgensen P, Olsen J, Jensen HJA (1988) J Chem Phys 74:265
46. Helgaker TU, Almlöf J, Jensen HJA, Jørgensen P (1986) J Chem Phys 84:6266
47. Helgaker TU, Taylor PR (1992) Unpublished
48. Jensen HJA, Jørgensen P, Ågren H, Olsen J (1988) J Chem Phys 88:3824
49. Roos BO, Andersson K, Fülscher MP (1992) Chem Phys Lett 192:5
50. McGlynn SP, Azumi T, Kinoshita M (1969) Molecular Spectroscopy of the Triple State. Prentice Hall, Engelwood Cliffs, NJ
51. Doering JP (1969) J Chem Phys 51:2866
52. The oscillator strengths are obtained with the *E*-factor given by the excitation energy to the $^3B_{1u}$ state as given by experiment (the MCLR energy deviates only minorly, see Table 1).
53. Rabalais JW, Maria HJ, McGlynn SP (1969) J Chem Phys 51:2259
54. van Egmond J, van der Waals JH (1973) Mol Phys 26:1147
55. Bendazolli GL, Palmieri P (1974) Int J Quant Chem 8:941
56. Langhoff SR, Davidson ER (1976) J Chem Phys 64:4699
57. Phillips P, Davidson ER (1982) J Chem Phys 86:3729
58. Colson SD, Bernstein ER (1965) J Chem Phys 43:2661
59. Wright MR, Frosch RP, Robinson GW (1960) J Chem Phys 33:934
60. Colson SD, Robinson GW (1968) J Chem Phys 48:2550
61. Johson PM, Koronowski GM (1983) Chem Phys Lett 97:53